# An integrated framework for high-resolution urban flood modelling considering multiple information sources and urban features

Yuntao Wang[a,b], Albert S. Chen[b], Guangtao Fu[b],

Slobodan Djordjević[b], Chi Zhang[a,*], Dragan A. Savić[b]

[a] School of Hydraulic Engineering, Dalian University of Technology, Dalian 116024, China

[b] Centre for Water Systems, College of Engineering, Mathematics and Physical Sciences, University of Exeter, North Park Road, Harrison Building, Exeter EX4 4QF, UK

*Corresponding author: Chi Zhang, E-mail address: czhang@dlut.edu.cn

Highlights

- New holistic framework is developed to handle multi-source data and urban features.
- Flood data from social media are a useful source for setting the model parameters.
- Urban micro-features can significantly influence simulated inundation extent and depth.
- Constant infiltration can better represent drainage capacity than the rainfall reduction approach in the study.
- This study provides an in-depth insight into high resolution urban flood modelling.

Abstract: High accuracy models are required for informed decision making in urban flood management. This paper develops a new holistic framework for using information collected from multiple sources for setting parameters of a 2D flood model. This illustrates the importance of identifying key urban features from the terrain data for capturing high resolution flood processes. A Cellular Automata based model CADDIES was used to simulate surface water flood inundation. Existing reports and flood photos obtained via social media were used to set model parameters

and investigate different approaches for representing infiltration and drainage system capacity in urban flood modelling. The results of different approaches to processing terrain datasets indicate that the representation of urban micro-features is critical to the accuracy of modelling results. The constant infiltration approach is better than the rainfall reduction approach in representing soil infiltration and drainage capacity, as it describes the flood recession process better. This study provides an in-depth insight into high resolution flood modelling.

Key words: CADDIES; DEM resolution; drainage capacity; flood modelling; multi-information; urban feature

## 1. Introduction

Urban flooding has become one of the most significant natural hazards due to climate change and rapid urbanization (Di Paola et al., 2014; Fu et al., 2011; Vacondio et al., 2016; Yang et al., 2016; Yin et al., 2016b). The growing trends of the frequency and the intensity of extreme rainfall events have increased the likelihood that the surface runoff overwhelms the drainage capacity. As a result, greater flood impacts to human society are expected to happen (Curebal et al., 2016; Korichi et al., 2016; Rosso and Rulli, 2002). For example, the July 2012 flood event in Beijing led to 79 deaths and an estimated economic loss of US$1.86 $\times 10^9$ (Yin et al., 2016a). To develop effective strategies for flood risk management, better understanding of flood dynamics is essential. In an urban area, not only the terrain elevation, but also the existence of artificial structures above the ground and the drainage network underground affect the runoff propagation significantly. Therefore, assessing the flood

movements in urban area requires a modelling approach that can reflect the influences of these factors.

Significant efforts have been made during the last few decades to improve accuracy and efficiency of urban flood modelling through enhanced methodology and numerical methods (Bates et al., 2010; Chen et al., 2007; Chen et al., 2010; Nguyen et al., 2006) and applications of parallel computing technologies (Ghimire et al., 2013; Glenis et al., 2013; Lamb et al., 2009; Smith and Liang, 2013). However, modelling accuracy is still affected by four main issues: 1) the level of details available in the topographic representations of terrain and urban key features (Haile and Rientjes, 2005; Horritt and Bates, 2001; Leandro et al., 2016; Rafieeinasab et al., 2015); 2) the lack of calibration and validation data (Fu et al., 2011; Hall et al., 2005; Horritt, 2000; Leandro et al., 2011); 3) the approach used to consider the effects of underground urban drainage infrastructure (drainage capacity) (Chen et al., 2009; Environment Agency, 2013b); and 4) the uncertainty of accelerated land use changes (De MOEL and Aerts, 2011; Du et al., 2015; Shi et al., 2007).

Micro urban features such as buildings, roads and underpasses can change the flow patterns and lead to erroneous simulation results (Allitt et al., 2009; Chen et al., 2012a; Chen et al., 2012b; Haile and Rientjes, 2005; Horritt and Bates, 2001; Priestnall et al., 2000; Vojinovic and Tutulic, 2009). For example, depending on how the buildings are represented in a model, the water may flow around buildings when the movement is restricted by building walls, or it may enter buildings when the water level exceeds the heights of their entrances. In recent years, the availability of Light

Detection and Ranging (LiDAR) data has enabled modelling using high resolution terrain data with a horizontal spatial resolution ranging from 0.25 m to 2 m and a vertical accuracy between 5 cm and 15 cm (Bates et al., 2003; Chen et al., 2012a; Deshpande, 2013). The improved quality of topographic datasets allows hydraulic models to better describe the flow dynamics affected by buildings in urban areas. The original LiDAR data - often in the form of a digital surface model (DSM), which includes buildings, trees, bridges over main roads and any other objects and features, can significantly influence the flow direction in modelling. Filtering algorithms are applied to produce a digital elevation model (DEM) that represents the ground surface only (Priestnall et al., 2000). Nevertheless, ability of a generic filtering procedure to capture the complex situations in an urban environment is limited, such that a better processing is necessary to build a suitable terrain model for urban flood simulations.

Pluvial flooding in urban areas often occurs rapidly such that it is difficult to obtain good measurements of flood extents and depths for model calibration and validation. To bridge this gap, multiple sources of information can be used, such as the existing reports or the historical flood extent maps, as an alternative approach to reconstruct an accurate representation of reality (Chau and Lee, 1991; Mark et al., 2014). Although satellite imagery was used for delineating flood extents and calibrating model parameters to simulate fluvial events (Di Baldassarre et al., 2009; Domeneghetti et al., 2014; Horritt, 2000; Mason et al., 2009; Matgen et al., 2004; Oberstadler et al., 1997), it is not feasible to implement such an approach for short-lived pluvial events. In another study, dendrogeomorphic evidence (i.e., scars on

trees) was used as benchmarks in roughness calibration (Ballesteros et al., 2011). In urban areas, the wide availability of smart phones, digital photos and social media provides an opportunity to obtain flood-related information where direct measurements are not available (René et al., 2015), which can support model verification. For example, platforms such as Twitter or crowd-sourcing web portals now carry a wealth of information regarding on-going or past flood events (Smith and Liang, 2013; Wang et al., 2018; Yu et al., 2016). However, most of the applications can only underpin the locations and timing of flooding, and require human labour to extract flood depth or extent information (Fohringer et al., 2015).

In recent years, computer vision has received increasing attention in many engineering studies, including water level measurement, sewer overflow monitoring, urban flood warning (Du et al., 2017; Narayanan et al., 2014; Ridolfi and Manciola, 2018; Yu and Hahn, 2010). For example, Du et al. (2017) put forward a new grey-scale image processing method for fluid edge analysis, which can overcome many of the inherent challenges of fluid-edge measurement. Yu and Hahn (2010) proposed a difference image based JPEG communication scheme and water level measurement scheme using sparsely sampled images in time domain.

The correct representation of the infiltration in permeable areas and the drainage capacity of the underground pipe system can significantly influence accuracy of urban surface flood modelling (Leandro et al., 2016). Without considering the soil infiltration and the function of drainage systems, the flood simulations may be less accurate. However, the availability of drainage network data is very limited in many

areas such that a new approach to account for the factor is needed. Several applications have proposed a discounted rainfall rate or a fixed infiltration rate to account for the influence of soil infiltration and drainage in urban flood modelling (Chang et al., 2015; Chen et al., 2009; Environment Agency, 2013b; Henonin et al., 2013).

This paper aims to present a new holistic framework for high resolution 2D urban flood modelling that utilizes information from multiple sources and takes into account the influences of critical urban features on flood propagation. The new framework integrates the methodology to address the key challenge in improving the accuracy of urban flood simulations, including extraction of flood information, handling of urban key feature and model assessment methods. More specifically, an original procedure is developed to extract flood inundation extent and depth from social media photographs collected during flood events, and cross-validated using terrain analysis. Urban key features such as building layouts and underpasses are identified using different terrain data sets. The confusion matrix is used as a model assessment approach to consider the impact of model uncertainties and determine the values of key parameters. In this paper, the Cellular Automata Dual-DraInagE Simulation (CADDIES) model (Guidolin et al., 2016) was applied to a case study in Wallington, London (UK), for comparison of two approaches for representing soil infiltration and drainage capacity. The storm event of 7 June 2016 was simulated to investigate how the urban feature representations in different terrain data settings affect flood modelling. The results obtained from the case study show the important

role of using multi-information sources in setting the parameters of the model, and the impact of urban key features on the performance of 2D flood simulation.

## 2. Methodology

Figure 1 summarizes the new framework developed in this study, which consists of three main components: DEM revision, flood information extraction, and flood modelling. These are explained in detail below.

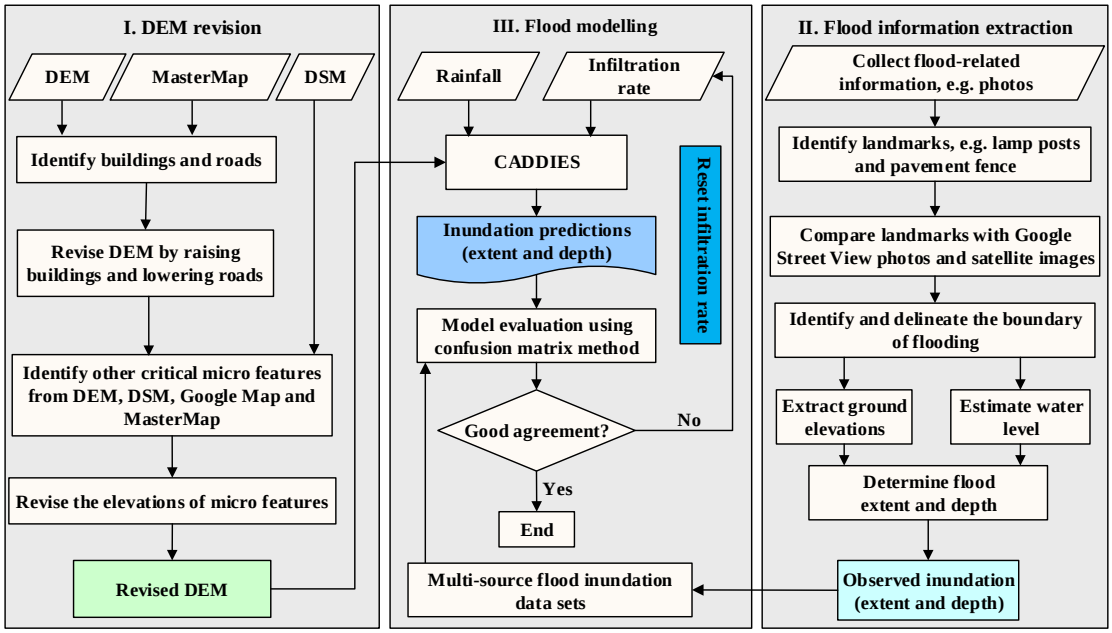


**Fig. 1.** The framework for high resolution urban flood modelling that considers the utilization of information from multiple sources and reflects the influences of critical urban features on flood propagation (DEM: digital elevation model, DSM: digital surface model)

### 2.1. Terrain data revision

As mentioned above, the generic DSM filtering algorithms for producing bare earth DEM has severe limitations in representing the actual urban environment. In the Environment Agency's (EA) surface water mapping, the terrain elevations of building footprints were raised by up to 0.3 m to reflect the floor level of buildings, while the elevations of roads were lowered by 0.125 m (Environment Agency, 2013b). We first

adopted the same approach, shown in Figure 1, to alter DEM for flood modelling and the results show a discrepancy with the filed observations. Therefore, we further investigated different thresholds for raising the terrain elevations of building footprints and other detailed modification to better present urban micro features in flood modelling.

(1) The topography polygon data from the Ordnance Survey MasterMap (2015) are converted into a land cover types map in raster format to identify the cells representing building footprints and roads.

(2) Both the raster files of DEM and land cover types overlapped such that the elevation data of building and road cells are revised accordingly.

(3) DSM is used to identify some other critical micro features, i.e., underpasses, by comparing their elevation differences between DEM and DSM, and also verifying the micro features through Google Map and MasterMap. The elevations of the cells, which represent these features, are further revised according to the real flow patterns near the key micro features.

**2.2. Reconstructing flood scenarios from multiple sources**

Although there were no detailed level or extent measurements at the location in Wallington during the 2016 flood event, many photos and videos were taken by the public and shared via social media or reported in the news. Most of the information were automatically time stamped via the devices or platforms being used. The flood information is manually processed in stages (Fig. 1).

(1) Related flood photos and videos at different timings during the event were

collected from social media and news websites.

(2) The landmarks near the flood boundary, such as lamp posts and pavement fences in the photos, were used as reference points to identify the boundary of the flood extent by comparing them to the Google Street View photos and satellite images. Then the locations of the boundary are determined using the Google Map service and geo-referenced in GIS.

(3) The ground elevations at those boundary points were extracted from LiDAR data and used as the water level to delineate the boundary of flooding, assuming the cells within the boundary with lower elevations were submerged during the event. The flood extent obtained from the terrain analysis was cross-validated again using the above data.

(4) Finally, water depths within the flood extent were obtained by subtracting the ground elevation of each cell from the water level extracted in step (3), and then inundation volume and area can be estimated. Furthermore, the inundation area and volume were calculated with simplified formulas (1) and (2), respectively, which are then used to compare with the simulation results:

$$S = N * \Delta s \tag{1}$$

$$V = \sum_{i=1}^{N} (h_w - h_i) \Delta s \tag{2}$$

Where $S$ is the inundation area, $\Delta s$ is the area of the cell, $N$ is the number of flooded cells, $h_w$ is the water level, $h_i$ is the ground elevation of each cell.

## 2.3. Accounting for infiltration and drainage capacity in urban flood modelling

The methods used to consider infiltration and drainage capacity in urban flood modelling are different (Chang et al., 2015; Leandro et al., 2009; Vojinovic and Tutulic, 2009). The highly efficient one-dimensional (1D) model is the most commonly used tool to simulate the hydraulic performance of urban drainage systems, and infiltration during the simulation process of the rainfall-runoff is usually calculated by using an additional module. For example, Storm Water Management Model (SWMM) provides choices for modeling infiltration, i.e., Horton Method and Green-Ampt Method. Leandro et al. (2016) introduced a modified Green-Ampt equation for handling compacted urban soils with limited storage capacity when modelling rainfall-runoff in urbanized areas. However, difficulties exist in obtaining drainage system data to build the sewer network model (Liu et al., 2015; Zhang and Pan, 2014). For example, in some cities, there is a lack of sufficient and accurate knowledge and data on the sewer system, such as pipe layout and diameters.

In this paper, two approaches, rainfall reduction and constant infiltration, were used to represent soil infiltration and urban drainage network capacity. In the rainfall reduction approach, a fixed percentage reduction is applied to the design rainfall before input to the model to reflect the infiltration and drainage capacity in urban areas, i.e., the design rainfall is reduced to represent infiltration over pervious areas and then a further reduction of rainfall is applied to represent the effect of the drainage system (Environment Agency, 2013a). In the constant infiltration approach, the soil infiltration and the function of sewer drainage system are represented as constant

infiltration rates in the 2D overland flow model. The design rainfall is applied directly onto the surface without any reduction.

### 2.4. Flood modelling using CADDIES

CADDIES is a fast 2D urban flood simulation model based on the principle of cellular automata (CA) (Ghimire et al., 2013; Gibson et al., 2016; Guidolin et al., 2016; Guidolin et al., 2012). This model's effectiveness has been proven on the EA's 2D benchmark test cases and real world case studies (Guidolin et al., 2016). In this paper, the DEM, DSM and revised DEM data were used as input to the CADDIES model to analyze the impact of terrain data on the simulation results.

### 2.5. Performance assessment

To evaluate the performance of various model settings, we adopted two indicators, the true positive rate (TPR) and positive predictive value (PPV) from a confusion matrix (Chang et al., 2015). A confusion matrix is a table with two rows and two columns, which shows the number of false positives, false negatives, true positives and true negatives, and can be used to calculate TPR, PPV, true negative rate and negative predictive rate. As flooded cells are concerned, so TPR and PPV are selected for use in this study and are calculated as below:

$$TPR = \frac{TP}{TP + FN} \tag{3}$$

$$PPV = \frac{TP}{TP + FP} \tag{4}$$

Where TP represents the number of cells for which the model correctly predicted flooding, FP is the number of cells incorrectly predicted as flooded, and FN denotes

the number of flooded cells that the model failed to predict correctly.

Higher TPR and PPV values indicate that the model better approximated the observed flooding. For example, the maximum TPR and PPV are 1 under the situation when FN and FP are equal to 0, i.e., the predicted flooding extent from the model is the same as the observed flooding.

This framework was applied to a case study in London using a high-performance desktop machine, which has an Intel Core i7-4770K CPU having four physical cores at 3.50 GHz, 32 GB of main memory and a Tesla K20c graphics card with 2496 CUDA cores and 5 GB of video memory. The use of the GPU approach significantly improved computational performance, while achieving required accuracy. For example, the simulation time for the study area (1 m x 1 m resolution) is less than 100 seconds, which enables flood modelling to be undertaken while considering a large number of scenarios, such as different storm events and different combinations of infiltration rates.

## 3. Case study

### 3.1. Study area

In this paper, the Wallington area in the London Borough of Sutton was used as the case study (Fig. 2). The topography data (Ordance Survey, 2015) was classified into six different land cover types, including building, green land, manmade surface, rail, road and road side areas, to set up the parameters for infiltration and roughness estimates. The total area is 0.25 $km^2$, 69.4% of which is occupied by buildings and impervious surfaces, while 30.6% of the area remains as permeable green land.

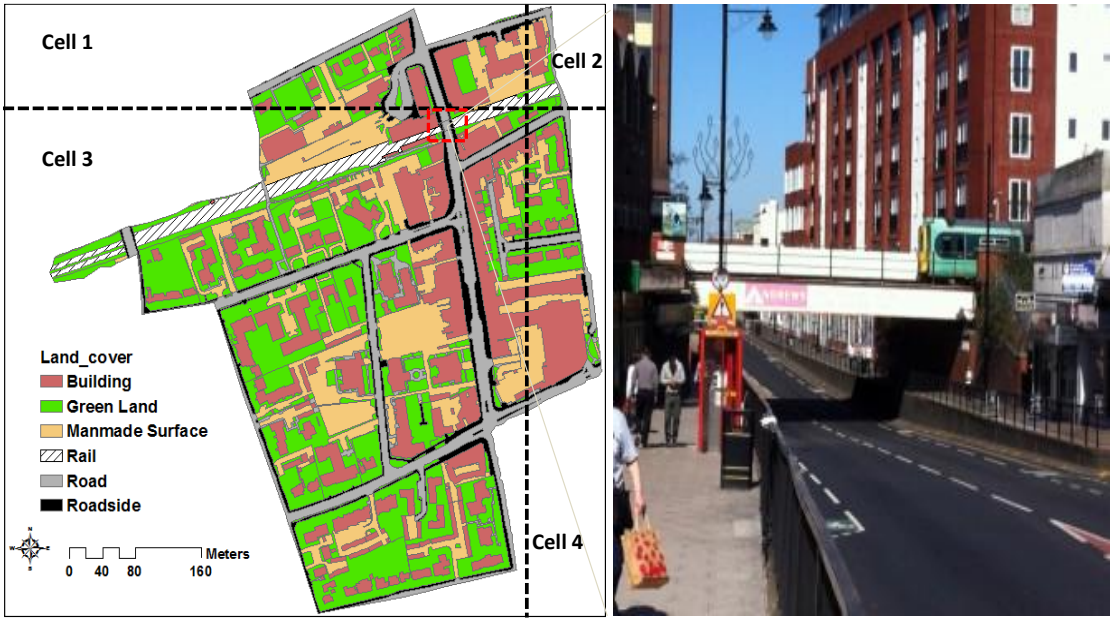


**Fig. 2.** Land cover of the study area and the image of the underpass during dry weather. Cells 1-4 (1 km x 1 km) are radar rainfall cells covering the study area.

Although there are no rivers or watercourses, Wallington has suffered flooding from pluvial events frequently. For example, 44 mm of rainfall fell on the morning of 20 July 2007 that overwhelmed the local drainage system such that the surface water flowed along the roads from the surrounding areas towards the underpass at Wallington Station (Sutton, 2010). Therefore, flooding in the Wallington Station Road Bridge area is due to a combination of insufficient capacity of the local drainage network and low-lying terrain.

### 3.2. Terrain data

The EA's 1 m resolution LiDAR DEM (bare terrain) and DSM (terrain with buildings and vegetation), with a vertical accuracy of ±0.15 m (Environment Agency, 2016), were used to represent the terrain elevation, as shown in Figs. 3(a) and (b).

Two approaches for revising the DEM were applied for modelling the building

blockage effect: 1) DEM I that the elevations of building footprints were raised by 0.3 m and roads were lowered by 0.125 m (Environment Agency, 2013b), and 2) DEM II that the elevations of building footprints were raised by 5.0 m and roads were lowered by 0.125 m, as shown in Figs. 3(c) and (d). These two approaches are in line with recommendations in literature (Environment Agency, 2013b; Vojinovic and Tutulic, 2009). The first approach assumes that the water can flow through the building once the depth exceeds the threshold height of 0.3 m, while the second approach literally forces the water to flow around buildings. Furthermore, several problems with DEM were resolved prior to modelling. For example, the difference between the elevation of the pavement and the road underpass is 1.5 m, but is not correctly represented in the DEM. Therefore, the elevations of the pavement at the underpass were also revised to provide an accurate digital representation.

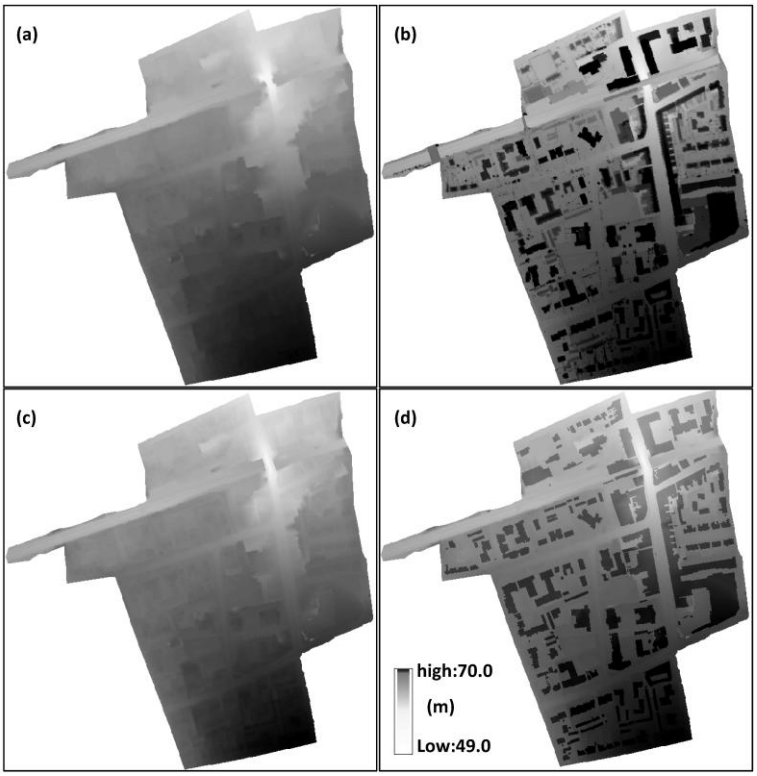


**Fig. 3.** DEM and DSM data of the study area. (a) 1 m x 1 m resolution DEM, (b) 1 m x 1 m

resolution DSM, (c) 1 m x 1 m resolution revised DEM I with roads lowered by 0.125 m and building blocks raised by 0.3 m, (d) 1 m x 1 m resolution revised DEM II with roads lowered by 0.125 m and building blocks raised by 5.0 m.

### 3.3. Drainage capacity

EA developed the updated Flood Map for Surface Water for England and Wales (Environment Agency, 2013a) with 2 m resolution using the hydraulic model JFlow + 2D (Bradbrook, 2006). In the EA's modelling, the design rainfall in the urban area was reduced by 30% to represent infiltration losses in pervious surfaces, and a fixed rate of rainfall reduction (for most cases, 12 mm/h was used as the fixed rate, but it was varied between 6 mm/h and 20 mm/h) was further applied to represent the effect of the drainage system, as shown in Fig. 4, before being input to the model to reflect the infiltration and drainage capacity in urban areas. Even though the released maps only provide the flood extent information, i.e., no detailed flood depths are given, they can be used as reference for evaluating CADDIES modelling results. This was performed using the exactly same rainfall treatment settings.

The rainfall reduction approach assumes that soil infiltration and drainage capacity are accounted for in the model indirectly via this simplified methodology. However, the flood tends to recede via the drainage pipe systems once the rainfall intensity is less than the sewer capacity. The rainfall reduction approach fails to correctly represent the process of flood evolution over time, thus a different approach was introduced. As CADDIES allows spatially varying infiltration rates to be specified for different land cover, different constant infiltration rates were applied to each land cover category (a constant infiltration approach, the same is in the EA

studies) to reflect both urban drainage capacity and soil infiltration.

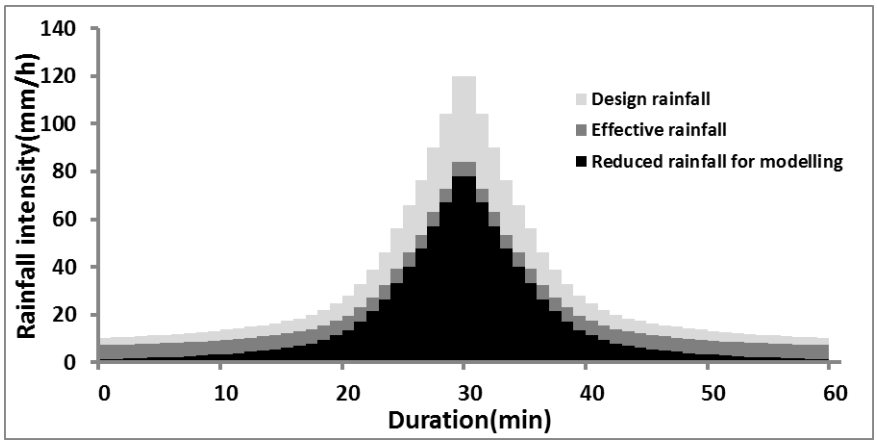


**Fig. 4.** Reduced rainfall approach for flood modelling.

### 3.4. Rainfall events

#### 3.4.1. Design rainfall events

The rainfall with three durations (1, 3 and 6 h) of 30, 100 and 1000 year return periods, using the Intensity-Duration-Frequency (IDF) curves from the Flood Estimation Handbook (FEH) (CEH, 2015), were modelled and compared to the EA's surface water mapping. However, after comparing the numerical simulation results of events of different durations with the same return period, we found that rainfall events of 1h duration consistently led to worse surface water flooding than events with longer durations, which was not surprising considering relatively small catchment (longest distance less than 1 km). The design rainfall depth of 1 hour and peak rainfall intensity (using a 2-minute time step) under different return periods are shown in Table 1.

**Table 1**

Rainfall depth and peak rainfall intensity of 1-hour design rainfalls for 30-, 100- and 1000-year return periods.

| Return period (year) | Rainfall depth (mm) | Peak rainfall intensity (mm/h) |
|---|---|---|
| 30 | 32 | 121 |
| 100 | 42 | 159 |
| 1000 | 69 | 263 |

### 3.4.2. The 7 June 2016 event

On 7 June 2016, a high intensity precipitation event lasting for 40 minutes caused flash flooding with more than 2 m water depth and three cars were completely submerged under the bridge on Wallington High Street.

The radar rainfall data were collected from the British Atmospheric Data Centre (BADC) archive, with spatial and temporal resolutions as 1 km and 5 minutes, respectively, and used as the input into the CADDIES model for this event. The study area is covered by four radar cells as shown in Fig. 2. Fig. 5 shows the rainfall hyetographs of the 7 June 2016 event for the four radar cells. The event began around 14:00 and lasted about 1.5 hours, and more than 90% of the rainfall occurred in the first 40 minutes. For example, the total rainfall registered in radar cell 1 during 1.5 hours was about 58 mm with the peak rainfall intensity of 163 mm/h, which occurred between 14:20 and 14:25.

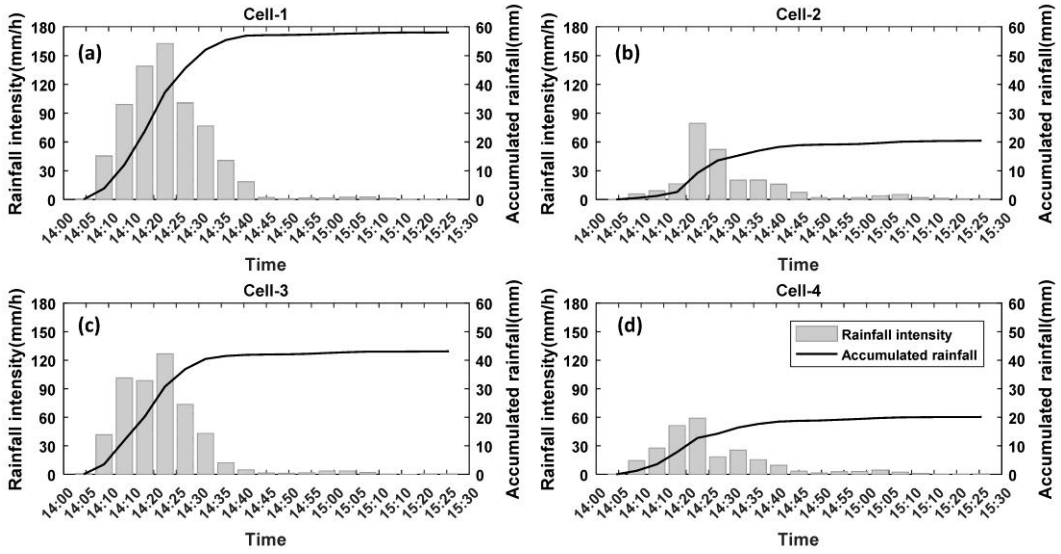


**Fig. 5.** The rainfall hyetographs of the 7 June 2016 event for the four cells in the study catchment (shown in Fig. 2).

### 3.5. Inundation data

Fig. 6(a), (b) and (c) show three photos collected from Twitter featuring the flood event in the area of Wallington station at 14:50 on 7 June 2016. The flood boundary was determined from these flood pictures. For example, as shown in Fig. 6(a) and (b), the signpost and pavement fence near the boundary line were identified in the photos as the reference points. By comparing these landmarks with the Google Street View photos and satellite images, the spatial relationship between the buildings and the landmarks can be identified, which helped delineate the boundary of the flooding. The water level was obtained using the elevation of the boundary. Assuming the horizon water level covering the neighbor areas with lower elevations, the flood extent was determined through terrain analysis as the red-outlined polygon shown in Fig. 6(d). Furthermore, the high resolution MasterMap information, including the detailed layouts of buildings, roads, and roadsides, were used to cross-validate the flood

boundary identified from terrain analysis. A water level of 51.4 m was determined at 14:50, and then the water depth of each cell was calculated by subtracting its ground elevation from the water level.

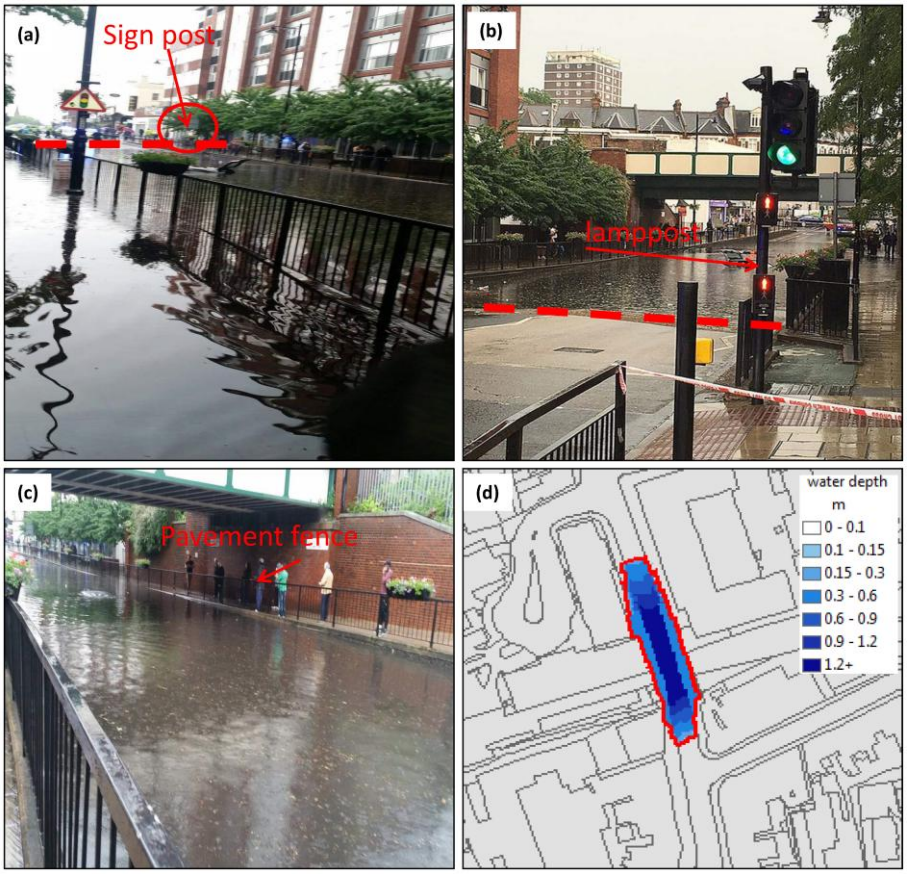


**Fig. 6.** The flood extent and depth near Wallington station at 14:50 on 7 June 2016 (Twitter@Sunil).

## 4. Results and discussion

### 4.1. Comparison with the EA results

We adopted the same approaches of building footprint treatment, rainfall reduction and roughness setting to the ones used in the EA's surface water mapping for comparing our modelling results. Variable Manning's roughness values were assigned to different land cover types: (1) 0.05 s/($m^{1/3}$) for the building areas; (2) 0.03 s/($m^{1/3}$) for green lands; (3) 0.025 s/($m^{1/3}$) for manmade surface areas; (4) 0.05 s/($m^{1/3}$)

for rails; and (5) 0.02 s/($m^{1/3}$) for roads, pavements (Environment Agency, 2013a).

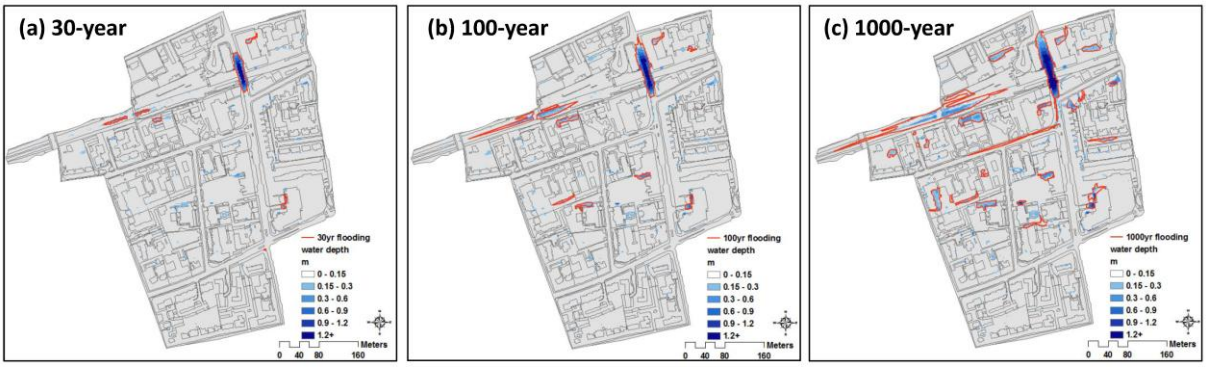


**Fig. 7.** Maximum flood depth of the study area obtained for the 30-, 100- and 1000-year design rainfall with the rainfall reduction approach. The red lines represent the flood extent obtained from the EA maps.

The spatial results for the maximum inundation extent and depth in the study area considering 30-, 100- and 1000-year return periods are presented in Fig. 7. The red lines represent the flood extents from the EA maps, extracted from the WMS service, and the blue shades represent the maximum water depths obtained by CADDIES. As expected, the underpass at Wallington station had the highest water depth of about 1.5 m. Thus, the simulation results of a sub-area underneath the Wallington station are highlighted and shown in detail. In the rainfall reduction approach, the CADDIES results show a good agreement between the modelled maximum inundation (extent and depth) and the EA results for all return periods when the drainage capacity was set to 6 mm/h, as shown in Figs. 8(a), (b) and (c). This demonstrates that CADDIES is capable of reproducing results that are in agreement with the ones obtained from the JFlow + 2D model.

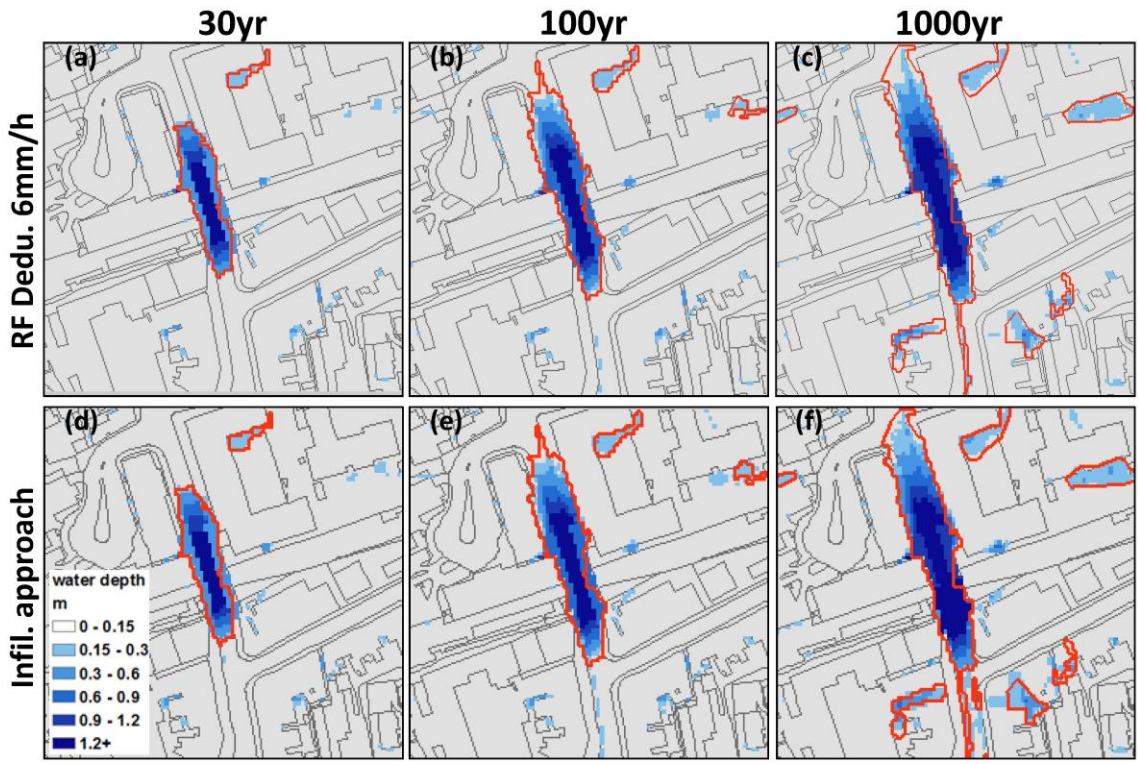


**Fig. 8.** Maximum flood depth in the underpass at Wallington station for the 30-, 100- and 1000-year design rainfall events using the rainfall reduction approach and constant infiltration approach. The red lines represent the flood extent from the EA maps.

The spatially variable infiltration rates were set and validated by comparing model predictions with the EA results using the rainfall reduction approach. Different combinations of infiltration rates were investigated, for example, the rate for green land use type was chosen from 15, 20, 25, 30, 35, 40 and 45 mm/h, and the rate for other layers, such as roads, manmade surfaces and similar areas was chosen from 10, 15, 20, 25 and 30 mm/h. TP, FP and FN in Wallington were counted by comparing the flood extent obtained from the model and the identified flood extent from the EA maps. The TPR and PPV were obtained from the 35 combinations of infiltration rates for 30-, 100- and 1000-year return periods. The resulting relationships between TPR and PPV are shown in Fig. 9. For example, each circle data point corresponds to one combination of the infiltration rate for the rainfall with the 30-year return period.

However, trade-offs exist between the two objectives, and even more extensive solution sets can be generated using various assumptions.

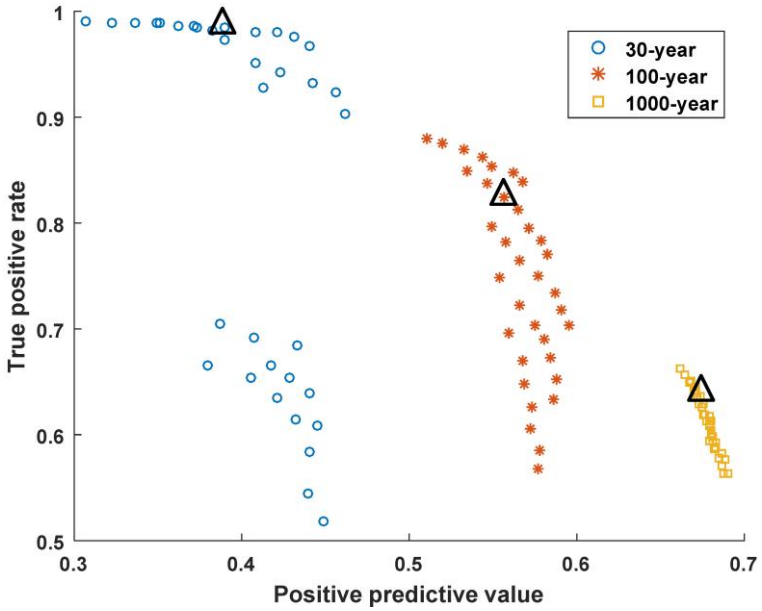


**Fig. 9.** True positive rate and positive predictive value for each combination of infiltration rates under the 30-, 100- and 1000-year design rainfall events. The triangles show the results of the combination of infiltration rates, i.e., 25 mm/h and 15 mm/h for the green land cover and other land covers, respectively.

In order to select the most appropriate combination of infiltration rates from the corresponding parameter sets in Fig. 9, we further compared the flood area of the underpass at Wallington station with the reported flood areas (1084 $m^2$, 1756 $m^2$, and 2280 $m^2$ for the 30-, 100- and 1000-year design rainfall events, respectively) from EA flood maps, as this is a critical area with potentially severe consequences. Table 2 shows the PPV, TPR and flood area of 4 combinations of infiltration rates. When using the combination of 25 mm/h and 15 mm/h, there are minimum differences between the flood areas obtained from the model and those from EA maps.

**Table 2** True positive rate, positive predictive value and flood area of underpass for 4 different combinations of infiltration rates under the 30-, 100- and 1000-year design rainfall events.

| Infiltration rates (mm/h) | | 30-year | | | 100-year | | | 1000-year | | |
|---|---|---|---|---|---|---|---|---|---|---|
| Green land | Other land covers | PPV | TPR | Area ($m^2$) | PPV | TPR | Area ($m^2$) | PPV | TPR | Area ($m^2$) |
| 20 | 10 | 0.32 | 0.99 | 1416 | 0.52 | 0.88 | 1916 | 0.66 | 0.66 | 2364 |
| 25 | 15 | 0.39 | 0.98 | 1264 | 0.56 | 0.82 | 1720 | 0.67 | 0.63 | 2320 |
| 30 | 10 | 0.35 | 0.99 | 1376 | 0.54 | 0.86 | 1872 | 0.67 | 0.64 | 2324 |
| 35 | 10 | 0.36 | 0.99 | 1356 | 0.55 | 0.85 | 1864 | 0.67 | 0.64 | 2348 |

As shown in Fig. 9 (triangles), a combination of infiltration rates, i.e., 25 mm/h and 15 mm/h for the green land cover and other land covers, respectively, were chosen using the confusion matrix analysis in combination with the inundation extent comparisons for the underpass at Wallington station. The results for the inundation extent obtained from the constant infiltration approach show a better agreement with the EA results, as shown in Figs. 8(d), (e) and (f), than the rainfall reduction approach.

In addition, the temporal evolution of flood volumes and areas for the study region and the underpass at Wallington station for a design rainfall of 30-year return period are presented in Fig. 10. The flood volumes during the first 30 minutes of the simulations are low for both approaches, and then they increase rapidly (the peak rainfall occurs at about 30 minutes from the start). The flood volume obtained using the constant infiltration approach begins to decrease after 60 minutes due to the continuous drainage. However, the flood volume obtained using the rainfall reduction approach stays relatively flat after reaching its peak because drainage is not allowed

in the model setting. The results demonstrate the approach using constant infiltration rate can better reflect the physical phenomena where the excess runoff is absorbed by the sewer system. But the peak volumes from both approaches are similar, for example, the maximum flood volumes are 1,643 $m^3$ and 1,784 $m^3$ for the constant infiltration and the rainfall reduction approaches, respectively. The flood area curves in Fig. 10(b) show a similar trend to the flood volume curves, and the maximum flood areas are 4,108 $m^2$ and 4,252 $m^2$, respectively.

Similarly to Figs. 10(a) and (b), the flood volumes and areas in the underpass at Wallington station under two different infiltration conditions, are shown in Figs. 10(c) and (d). The flood volume and area from the rainfall reduction approach show the same trends as with the entire study area. However, the changes for the constant infiltration approach are slow because the limited inlet drainage capacity cannot quickly drain away the amount of ponding water that has concentrated into the area. The peak values of volume and area obtained using both approaches are similar, i.e., the maximum flood volume and area from constant infiltration and the rainfall reduction approaches are 984 $m^3$ and 1308 $m^2$, and 1080 $m^3$ and 1360 $m^2$, respectively.

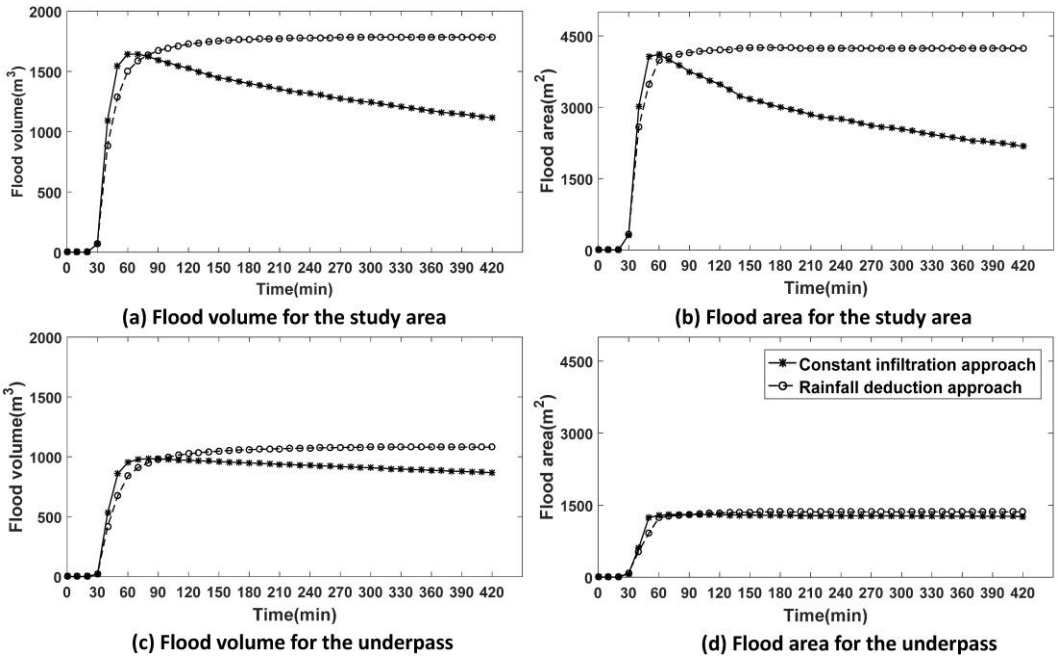


**Fig. 10.** Flood volume and area over time for the 30-year return period rainfall with the constant infiltration approach and rainfall reduction approach. (a) and (b) for the entire study area, (c) and (d) for the underpass at Wallington station, respectively.

### 4.2. The impact of terrain data

To investigate the influence of the terrain data on flood simulation results at Wallington station, four different terrain data versions described earlier (i.e. DEM, DSM, DEM I and DEM II) with the grid size of 1 m x 1 m were used. Spatially varied rainfall hyetographs were applied to different parts of the catchment covered by four radar cells in CADDIES. Fig. 11 shows the modelled inundation depth and extent results at 14:50 on 7 June 2016, which can be compared to the inundation identified from the photos in Fig. 6. Furthermore, the identified inundation volume and area calculated with simplified formulas (1) and (2) are 1,023 $m^3$ and 1,285 $m^2$.

The use of the bare DEM results in a significant loss of urban feature information, such as buildings and roads. As shown in Fig. 11(a), the flood extent is larger than that estimated from the photos and there is flooding inside buildings. This

is because the water can flow over the building layer when using the DEM data for modelling. However, the photos in Fig. 6 show no flooding inside buildings. Clearly, output is affected to a large extent by the bare DEM without considering the blockage effect of buildings. The DSM data includes terrain features, such as road and railway embankments, bridges and tunnels, which may change flow paths and can influence the flood evolution over time (Vacondio et al., 2016). For example, as shown in Fig. 11(b), the flood was divided into two parts by the railway bridge. Thus, topography is one of the critical factors affecting the simulation results. In order to achieve a satisfactory output, terrain data were revised to achieve correct description of these important features.

Fig. 11(c) and (d) show the inundation depth and extent obtained using DEM I and DEM II. The main difference between the two DEMs is the building height raised to reflect the blockage effect, i.e., 0.3 m or 5.0 m. The flood volume and area of the underpass at Wallington station with DEM I are 2,137 $m^3$ and 2,113 $m^2$, respectively. They are, however, 1,894 $m^3$ and 1,932 $m^2$, respectively for DEM II. The simulation results show that the inundation obtained using DEM I terrain data is larger than that with DEM II. However, the results obtained using DEM II are closer to observations, so they are considered better than those obtained with DEM I. This is particularly relevant to the treatment of buildings in high resolution urban flood modelling. The building height used DEM I is 0.3 m, so the flow through buildings is allowed to occur once the depth exceeds the assumed depth threshold. This confirms the finding that the raised building height has an effect on simulation results (Environment

Agency, 2013b).

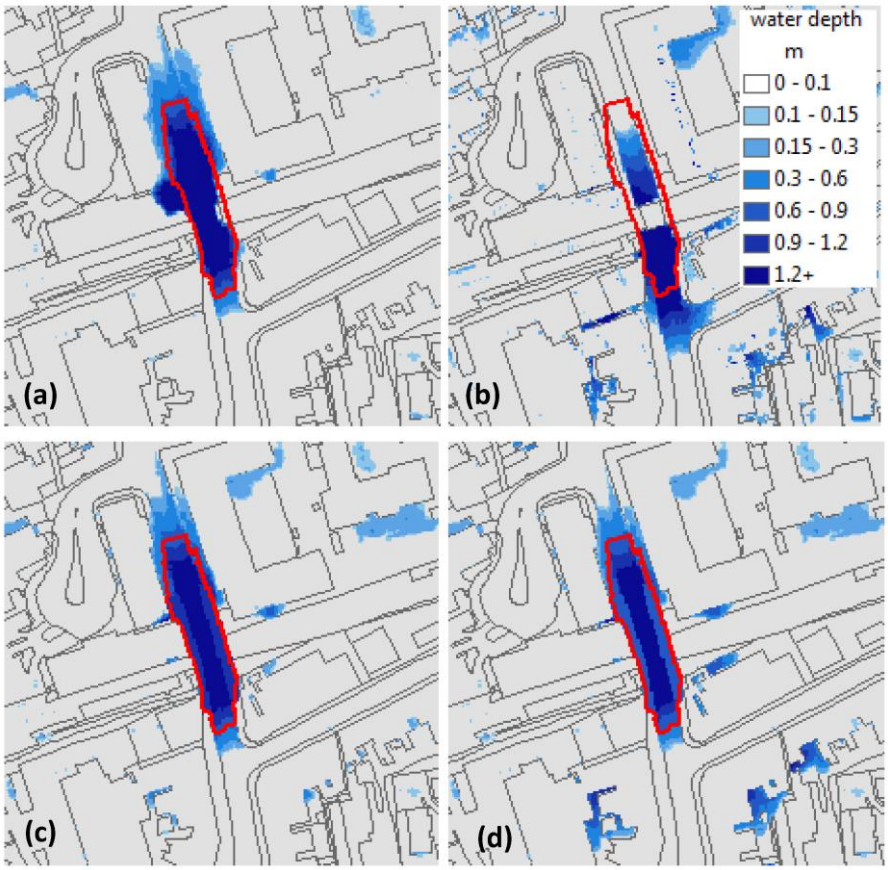


**Fig. 11.** The modelled inundation (extent and depth) at Wallington station at 14:50 on 7 June 2016 by using different terrain data, (a) the original bare DEM, (b) the DSM, (c) the revised DEM I with the building blocks raised by 0.3 m, and (d) the revised DEM II with the building blocks raised by 5.0 m. The red boundary line represents the observed flood areas at 14:50 on 7 June 2016.

### 4.3. The impact of drainage capacity

As discussed above, the combination of constant infiltration rates of 25 mm/h and 15 mm/h for green land and other land covers, respectively, was selected to get similar results with the EA study. However, when we applied that scenario to the 7 June 2016 event, the modelled results showed differences from the inundation identified from collected photos, i.e., it was larger than the identified inundation, which indicated that the infiltration rates used in the model could be lower than the

real drainage capacity. Therefore, three more scenarios of infiltration rates were chosen for further impact analysis of drainage capacity: 'Infiltration I' with 30 and 20 mm/h; 'Infiltration II' with 40 and 30 mm/h; and 'Infiltration III' with 50 and 40 mm/h, with the first value used for the green land and the second for other land covers. The flood maps at Wallington station under different infiltration scenarios are shown in Fig. 12, and all these flood maps were obtained with terrain data of DEM II.

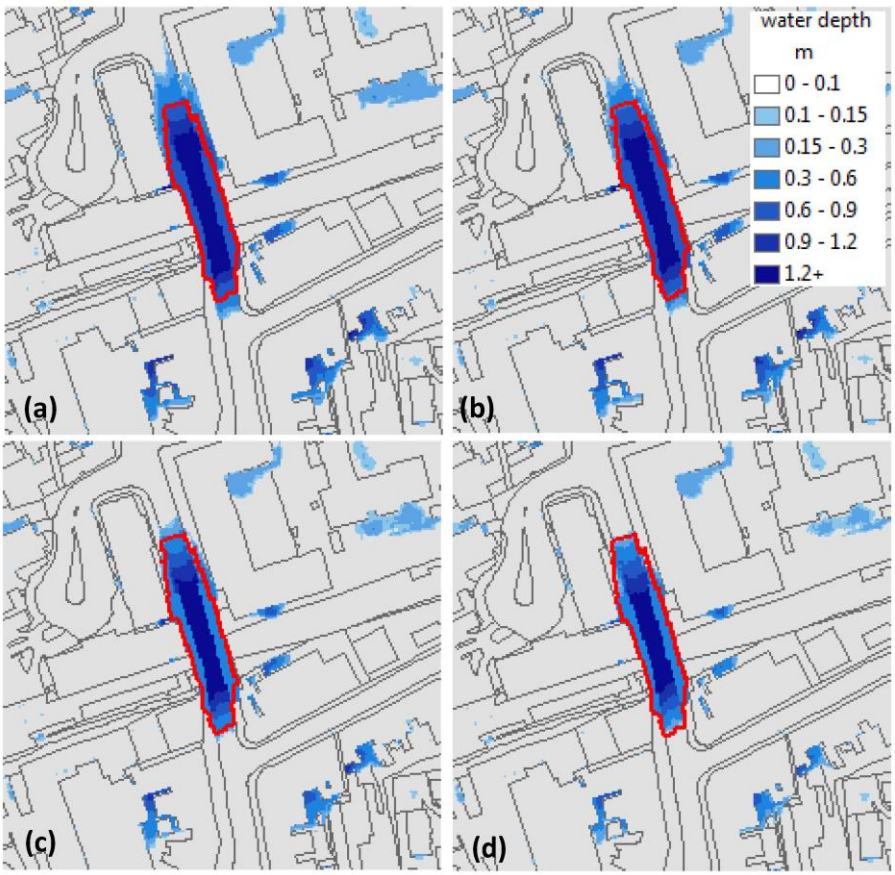


**Fig. 12.** The modelled inundation (extent and depth) at Wallington station at 14:50 on 7 June 2016 by using different sets of infiltration rates, (a) 25 mm/h and 15 mm/h, (b) 30 mm/h and 20 mm/h, (c) 40 mm/h and 30 mm/h and (d) 50 mm/h and 40 mm/h. The red boundary line represents the flood areas at 14:50 on 7 June 2016.

Table 3 shows the resulting inundation (volume and area) for the underpass at 14:50 for the simulations using the different drainage capacity scenarios. The

inundation volume and area for the underpass gradually reduce with increasing drainage capacity, i.e., 1894, 1686, 1314 and 1014 $m^3$ for the scenarios as 'Infiltration', 'Infiltration I', 'Infiltration II' and 'Infiltration III', respectively. The results show that the 'Infiltration III' produced the flood volume and area by far closest to observations, with minor differences of 9 $m^3$ and 87 $m^2$ (0.9% and 6.8%) respectively.

**Table 3** Inundation volume and area for the underpass at Wallington station at 14:50 on 7 June 2016 from photos and modelled by using different infiltration rate scenarios.

| | Estimated | 'Infiltration' | 'Infiltration I' | 'Infiltration II' | 'Infiltration III' |
|---|---|---|---|---|---|
| Volume ($m^3$) | 1023 | 1894 | 1686 | 1314 | 1014 |
| Area ($m^2$) | 1285 | 1932 | 1788 | 1546 | 1372 |

Finally, the scenario of 'Infiltration III' settings is used with the design rainfall of 30-, 100- and 1000-year return periods. Fig. 13 shows that the modelled flood extent estimates for different return periods are smaller than that from the EA study values. The results indicate that the drainage capacity in the EA study might be underestimated, which is also supported by the EA's latest review of approaches to represent drainage capacity for surface water mapping (Environment Agency, 2017).

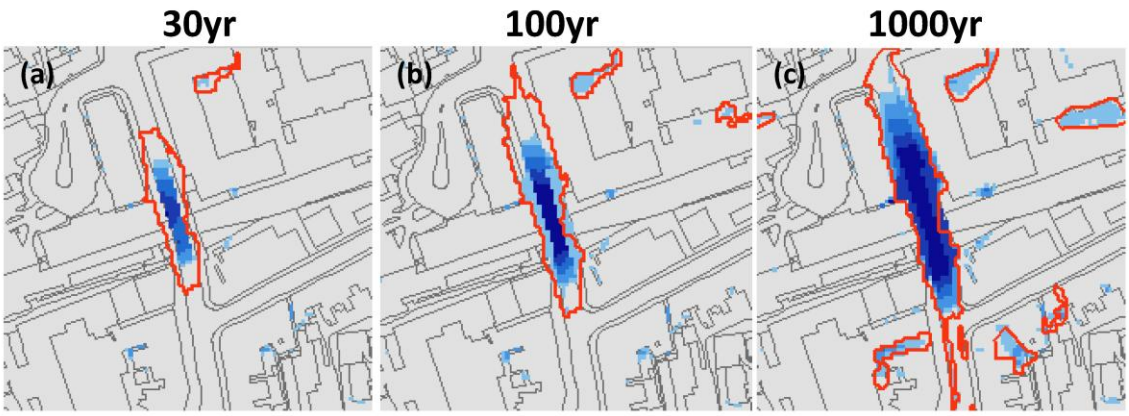


**Fig. 13.** Maximum flood depth of the underpass at Wallington station under the 30-, 100- and 1000-year design rainfall with infiltration sets of 50 mm/h and 40mm/h. The red lines represent the flood extent from the EA's map.

## 5. Conclusions

In this paper a holistic framework was developed to utilize the publicly available data to extract flood-related information for model calibration and validation. The proposed procedure allows the cross-validation of the derived data that improves the quality and reliability of the information. We also compared different parameter settings to investigate how to represent the influences of urban key features on flood propagations in high resolution modelling approach. Two methods, rainfall reduction and constant infiltration, were investigated and compared to reflect the soil infiltration and urban drainage network capacity when those information sources are absent. Furthermore, the impact of four different methods for extracting relevant terrain data was investigated through numerical simulations. The framework was tested on a case study of the Wallington (London) storm event on 7 June 2016. Specifically, the following conclusions could be drawn.

(1) The identified flood information obtained from social media is a useful

source for setting the model parameters.

(2) Two approaches for representing soil infiltration and drainage capacity, which were tested in this work, lead to different flood evolution results. The results of the rainfall reduction approach are not capable of reproducing in full the expected behaviour where the flood volume and area recede gradually after the flood peak occurs. The constant infiltration approach can describe the recession process better and should therefore be used for urban flood modelling.

(3) Urban micro-features, including buildings and underpasses, have significant influence on the inundation extent and depth. The results from the study suggest the building height should be raised by 5.0 m and the underpass elevations should be revised according to the actual flow condition.

This analysis improves understanding of urban flood processes and helps decision-making in flood risk management. Even though this study is developed for a small area, the knowledge generated from the CADDIES application can be scaled up to the city scale application by addressing the basic questions of how to set different drainage capacity and how to identify the important urban features in a large-scale terrain data. An automatic methodology for extracting flood information from photos should be further developed and we will study this in the future. Furthermore, many 1D/2D coupled models have been developed in recent years (Chen et al., 2007; Leandro et al., 2009), which can be used for identifying which of the simplified approaches for taking into account infiltration for urban flood modelling. There is a need to further compare the results of 1D/2D with the 2D models using the rainfall

reduction and constant infiltration approaches.

**Acknowledgments**

This research was partially funded by the British Council through the Global Innovation Initiative (GII206), the UK Engineering and Physical Sciences Research Council under the Building Resilience into Risk Management project (EP/N010329/1), and the SINATRA project of the NERC Flooding From Intense Rainfall programme (NE/K008765/1). The first author was funded by the China Scholarship Council. The authors would also like to thank the UK Environment Agency for the LIDAR datasets, UK Met Office (BADC) for the Radar rainfall data, Ordnance Survey for the Master Maps, and NVIDIA Corporation for the Tesla K20c GPU used in this research.

**Software availability**

Name of software: CADDIES-caflood

Developers: Michele Guidolin, Albert S. Chen, et al.

Contact address: Centre for Water Systems, College of Engineering, Mathematics and Physical Sciences, University of Exeter, Harrison Building, North Park Road, Exeter, EX4 4QF, UK

Email: A.S.Chen@exeter.ac.uk

Software required: OpenMP/OpenCL libraries

Hardware required: Multi-core CPU or OpenCL capable graphics card GPU

Programming language: C/C++, OpenCL

Program size: Around 20 MB

Availability: Open source MIT license

## References


Allitt, R., Blanksby, J., Djordjević, S., Maksimović, Č., Stewart, D., 2009. Investigations into 1D-1D and 1D-2D Urban Flood Modelling, WaPUG Autumn Conference.

Ballesteros, J., Bodoque, J., Díez-Herrero, A., Sanchez-Silva, M., Stoffel, M., 2011. Calibration of floodplain roughness and estimation of flood discharge based on tree-ring evidence and hydraulic modelling. J. Hydrol., 403(1): 103-115.

Bates, P., Marks, K., Horritt, M., 2003. Optimal use of high‐resolution topographic data in flood inundation models. Hydrol. Process., 17(3): 537-557.

Bates, P.D., Horritt, M.S., Fewtrell, T.J., 2010. A simple inertial formulation of the shallow water equations for efficient two-dimensional flood inundation modelling. J. Hydrol., 387(1): 33-45.

Bradbrook, K., 2006. JFLOW: a multiscale two‐dimensional dynamic flood model. Water and Environment Journal, 20(2): 79-86.

CEH, 2015. FEH Web Service. https://fehweb.ceh.ac.uk/.

Chang, T.-J., Wang, C.-H., Chen, A.S., 2015. A novel approach to model dynamic flow interactions between storm sewer system and overland surface for different land covers in urban areas. J. Hydrol., 524: 662-679. DOI:http://dx.doi.org/10.1016/j.jhydrol.2015.03.014

Chau, K.W., Lee, J.H.W., 1991. A microcomputer model for flood prediction with applications. Computer‐Aided Civil and Infrastructure Engineering, 6(2): 109-121.

Chen, A.S. et al., 2009. Pluvial flood modelling of the South East London resilience zone in the community resilience to extreme weather (CREW) Project, Flood And Coastal Risk Management Conference.

Chen, A.S., Djordjevic, S., Leandro, J., Savic, D., 2007. The urban inundation model with bidirectional flow interaction between 2D overland surface and 1D sewer networks, NOVATECH 2007, Lyon, France, pp. 465-472.

Chen, A.S., Djordjević, S., Leandro, J., Savić, D., 2010. An analysis of the combined consequences of pluvial and fluvial flooding. Water Science and Technology, 62(7): 1491-1498.

Chen, A.S., Evans, B., Djordjević, S., Savić, D.A., 2012a. A coarse-grid approach to representing building blockage effects in 2D urban flood modelling. J. Hydrol., 426: 1-16.

Chen, A.S., Evans, B., Djordjević, S., Savić, D.A., 2012b. Multi-layered coarse grid modelling in 2D urban flood simulations. J. Hydrol., 470: 1-11.

Curebal, I., Efe, R., Ozdemir, H., Soykan, A., Sönmez, S., 2016. GIS-based approach for flood analysis: case study of Keçidere flash flood event (Turkey). Geocarto International, 31(4): 355-366.

De MOEL, H., Aerts, J., 2011. Effect of uncertainty in land use, damage models and inundation depth on flood damage estimates. Natural Hazards, 58(1): 407-425.

Deshpande, S.S., 2013. Improved Floodplain Delineation Method Using High‐Density LiDAR Data. Computer‐Aided Civil and Infrastructure Engineering, 28(1): 68-79.

Di Baldassarre, G., Schumann, G., Bates, P.D., 2009. A technique for the calibration of hydraulic models using uncertain satellite observations of flood extent. J. Hydrol., 367(3): 276-282.

Di Paola, F. et al., 2014. Analysis of catania flash flood case study by using combined microwave and infrared technique. Journal of Hydrometeorology, 15(5): 1989-1998.

Domeneghetti, A. et al., 2014. The use of remote sensing-derived water surface data for hydraulic

model calibration. Remote Sensing of Environment, 149: 130-141.

Du, H., Li, M., Meng, J., 2017. Study of fluid edge detection and tracking method in glass flume based on image processing technology. Advances in Engineering Software, 112: 117-123.

Du, S., Van Rompaey, A., Shi, P., 2015. A dual effect of urban expansion on flood risk in the Pearl River Delta (China) revealed by land-use scenarios and direct runoff simulation. Natural Hazards, 77(1): 111-128.

Environment Agency, 2013a. Updated Flood Map for Surface Water-National Scale Surface Water Flood Mapping Methodology, Bristol, UK.

Environment Agency, 2013b. What is the updated Flood Map for Surface Water?(No. Report version 1.0), Bristol, UK.

Environment Agency, 2016. Environment Agency LIDAR data, Bristol, UK.

Environment Agency, 2017. Improving Surface Water Flood Mapping Work Package 1 - Drainage Rates (unpublished).

Fohringer, J., Dransch, D., Kreibich, H., Schröter, K., 2015. Social media as an information source for rapid flood inundation mapping. Natural Hazards & Earth System Sciences, 3(3): 4231–4264.

Fu, G., Butler, D., Khu, S.T., Sun, S.A., 2011. Imprecise probabilistic evaluation of sewer flooding in urban drainage systems using random set theory. Water Resour. Res., 47(2): W02534.

Ghimire, B. et al., 2013. Formulation of a fast 2D urban pluvial flood model using a cellular automata approach. J. Hydroinform., 15(3): 676-686.

Gibson, M.J. et al., 2016. Accuracy and Computational Efficiency of 2D Urban Surface Flood Modelling Based on Cellular Automata. Procedia Engineering, 154: 801-810. DOI:http://dx.doi.org/10.1016/j.proeng.2016.07.409

Glenis, V., McGough, A.S., Kutija, V., Kilsby, C., Woodman, S., 2013. Flood modelling for cities using Cloud computing. Journal of Cloud Computing: Advances, Systems and Applications, 2(1): 7.

Guidolin, M. et al., 2016. A weighted cellular automata 2D inundation model for rapid flood analysis. Environmental Modelling & Software, 84(2016): 378-394.

Guidolin, M. et al., 2012. CADDIES: A new framework for rapid development of parallel cellular automata algorithms for flood simulation, Proceedings of the 10th International Conference on Hydroinformatics (HIC 2012), Hamburg, Germany.

Haile, A.T., Rientjes, T., 2005. Effects of LiDAR DEM resolution in flood modelling: a model sensitivity study for the city of Tegucigalpa, Honduras. ISPRS WG III/3, III/4, 3: 12-14.

Hall, J., Tarantola, S., Bates, P., Horritt, M., 2005. Distributed sensitivity analysis of flood inundation model calibration. Journal of Hydraulic Engineering, 131(2): 117-126.

Henonin, J., Russo, B., Mark, O., Gourbesville, P., 2013. Real-time urban flood forecasting and modelling–a state of the art. J. Hydroinform., 15(3): 717-736.

Horritt, M., Bates, P., 2001. Effects of spatial resolution on a raster based model of flood flow. J. Hydrol., 253(1): 239-249.

Horritt, M.S., 2000. Calibration of a two‐dimensional finite element flood flow model using satellite radar imagery. Water Resour. Res., 36(11): 3279-3291.

Korichi, K., Hazzab, A., Atallah, M., 2016. Flash floods risk analysis in ephemeral streams: a case study on Wadi Mekerra (northwestern Algeria). Arabian Journal of Geosciences, 9(11): 589.

Lamb, R., Crossley, M., Waller, S., 2009. A fast two-dimensional floodplain inundation model. PROCEEDINGS OF THE INSTITUTION OF CIVIL ENGINEERS-WATER MANAGEMENT,

162(6): 363-370.

Leandro, J., Chen, A.S., Djordjević, S., Savić, D.A., 2009. Comparison of 1D/1D and 1D/2D coupled (sewer/surface) hydraulic models for urban flood simulation. Journal of hydraulic engineering, 135(6): 495-504.

Leandro, J., Djordjević, S., Chen, A.S., Savić, D.A., Stanić, M., 2011. Calibration of a 1D/1D urban flood model using 1D/2D model results in the absence of field data. Water Sci. Technol., 64(5): 1016.

Leandro, J., Schumann, A., Pfister, A., 2016. A step towards considering the spatial heterogeneity of urban key features in urban hydrology flood modelling. J. Hydrol., 535: 356-365.

Liu, L. et al., 2015. Developing an effective 2-D urban flood inundation model for city emergency management based on cellular automata. Natural Hazards & Earth System Sciences, 2(3): 6173-6199.

Mark, O. et al., 2014. Report and papers with guidelines on calibration of urban flood models, CORFU Project deliverable D2.2.

Mason, D.C., Bates, P., Dall'Amico, J., 2009. Calibration of uncertain flood inundation models using remotely sensed water levels. J. Hydrol., 368(1): 224-236.

Matgen, P. et al., 2004. Uncertainty in calibrating flood propagation models with flood boundaries derived from synthetic aperture radar imagery. Proc. 20th Congr. Int. Soc. Photogramm. Remote Sens., Istanbul, Turkey: 352-358.

Narayanan, R., Lekshmy, V., Rao, S., Sasidhar, K., 2014. A novel approach to urban flood monitoring using computer vision, Computing, Communication and Networking Technologies (ICCCNT), 2014 International Conference on. IEEE, pp. 1-7.

Nguyen, D.K., Shi, Y.-E., Wang, S.S., Nguyen, T.H., 2006. 2d shallow-water model using unstructured finite-volumes methods. Journal of Hydraulic Engineering, 132(3): 258-269.

Oberstadler, R., Hönsch, H., Huth, D., 1997. Assessment of the mapping capabilities of ERS‐1 SAR data for flood mapping: a case study in Germany. Hydrol. Process., 11(10): 1415-1425.

Ordance Survey, 2015. OS MasterMap Topography Layer [FileGeoDatabase geospatial data], Scale 1:1250, Tiles: GB, Updated: 11 June 2015, Ordnance Survey (GB), Using: EDINA Digimap Ordnance Survey Service, http://digimap.edina.ac.uk, Downloaded: 2016-02-02.

Priestnall, G., Jaafar, J., Duncan, A., 2000. Extracting urban features from LiDAR digital surface models. Computers, Environment and Urban Systems, 24(2): 65-78.

Rafieeinasab, A. et al., 2015. Toward high-resolution flash flood prediction in large urban areas–Analysis of sensitivity to spatiotemporal resolution of rainfall input and hydrologic modeling. J. Hydrol., 531: 370-388.

René, J.R. et al., 2015. A real‐time pluvial flood forecasting system for Castries, St. Lucia. Journal of Flood Risk Management, 11: S269-S283.

Ridolfi, E., Manciola, P., 2018. Water Level Measurements from Drones: A Pilot Case Study at a Dam Site. Water, 10(3): 297.

Rosso, R., Rulli, M.C., 2002. An integrated simulation method for flash-flood risk assessment: 2. Effects of changes in land-use under a historical perspective. Hydrology and Earth System Sciences Discussions, 6(2): 285-294.

Shi, P.-J. et al., 2007. The effect of land use/cover change on surface runoff in Shenzhen region, China. Catena, 69(1): 31-35.

Smith, L.S., Liang, Q., 2013. Towards a generalised GPU/CPU shallow-flow modelling tool.

Computers & Fluids, 88(12): 334-343.

Sutton, L.B.o., 2010. Surface Water Management Plan, Phase I & II – Final Report.

Vacondio, R., Aureli, F., Ferrari, A., Mignosa, P., Dal Palù, A., 2016. Simulation of the January 2014 flood on the Secchia River using a fast and high-resolution 2D parallel shallow-water numerical scheme. Natural Hazards, 80(1): 103-125.

Vojinovic, Z., Tutulic, D., 2009. On the use of 1D and coupled 1D-2D modelling approaches for assessment of flood damage in urban areas. Urban Water J., 6(3): 183-199.

Wang, R.Q., Mao, H., Wang, Y., Rae, C., Shaw, W., 2018. Hyper-resolution monitoring of urban flooding with social media and crowdsourcing data. Computers & Geosciences, 111(2): 139-147.

Yang, L. et al., 2016. Structure and evolution of flash flood producing storms in a small urban watershed. Journal of Geophysical Research: Atmospheres, 121(7): 3139-3152.

Yin, J., Yu, D., Wilby, R., 2016a. Modelling the impact of land subsidence on urban pluvial flooding: A case study of downtown Shanghai, China. Science of The Total Environment, 544: 744-753.

Yin, J., Yu, D., Yin, Z., Liu, M., He, Q., 2016b. Evaluating the impact and risk of pluvial flash flood on intra-urban road network: A case study in the city center of Shanghai, China. J. Hydrol., 537: 138-145.

Yu, D., Yin, J., Liu, M., 2016. Validating city-scale surface water flood modelling using crowd-sourced data. Environmental Research Letters, 11(12): 124011.

Yu, J., Hahn, H., 2010. Remote Detection and Monitoring of a Water Level Using Narrow Band Channel. J. Inf. Sci. Eng., 26(1): 71-82.

Zhang, S., Pan, B., 2014. An urban storm-inundation simulation method based on GIS. J. Hydrol., 517: 260-268.